March 2002

ELSEVIER

Materials Letters 53 (2002) 91–101

MATERIALS LETTERS

www.elsevier.com/locate/matlet

Impedance spectroscopy study of nickel electrodeposits

H.S. Karayianni [a,*], G.S. Patermarakis [a], J.C. Papaioannou [b]

[a] *Section of Materials Science and Engineering, Department of Chemical Engineering, National Technical University of Athens, Iroon Polytechniou 9, Zografou 157 80, Athens, Greece*

[b] *Laboratory of Physical Chemistry, Department of Chemistry, University of Athens, Panepistimioupolis 157 71, Athens, Greece*

Received 28 August 2000; received in revised form 19 June 2001; accepted 21 June 2001

Abstract

Nickel electrodeposits prepared in $NiSO_4$ and $NiCl_2$ electrolytes with thicknesses of 43–49.4 μm were examined by the impedance spectroscopy (IS) method for a–c frequencies 1 Hz–100 kHz. The Nyquist diagrams were single, almost perfect semicircles, suggesting the applicability of the in parallel combination of the R_a–C_a elements characterised by a single relaxation time, 8.27×10^{-6} s, combined in series with another R_b element, $R_b \ll R_a$. This relaxation time predicted that the incorporated hydrogen atoms are involved in the process of conduction by a hopping/diffusion mechanism, which is differentiated in the cases of $NiSO_4$–Ni and $NiCl_2$–Ni deposits. The diffusion coefficient of hydrogen, 1.25×10^{-11} cm^2 s^{-1}, was determined. The microstructure of Ni electrodeposits was also studied and characterised by electron microscopy. Finally, a general model for the microstructure of Ni electrodeposits, consistent with the results of impedance spectroscopy, was formulated.

Keywords: Nickel electrodeposits; Impedance spectroscopy; Hydrogen hopping/diffusion conduction mechanism; Microstructure model

1. Introduction

The selective orientation or the texture axis of nickel electrodeposits [1–4] and their secondary structure and morphology [4–6] were previously investigated. These samples prepared in pure $NiCl_2$ and $NiSO_4$ were examined in detail by the XRD, electron microscopy and optical microscopy methods [4]. From the mechanism of Ni deposition [4] and earlier results [7–13], the SO_4^{2-} [4,7], H and H_2 [8,9] and most probably H_2O (as molecular H_2O or as H^+ and OH^-) species are embodied in the $NiSO_4$–Ni deposits, while the Cl^- and Cl_2 [10,11], H, H_2 as well as OH^- (as $Ni(OH)_2$, $Ni(OH)^+$ and NiOH) and H_2O (as molecular H_2O or as H^+ and OH^-) [9–13] species are embodied in the $NiCl_2$–Ni deposits. The grain sizes and the amount of the incorporated species are affected by pH and especially by the current density [4]. The behaviour of Ni deposits in different corrosive environments [14,15], their sorptive properties [16,17], hardness [18] and protective properties [19] were also investigated.

The revealed nature/composition and structure of Ni deposits [1–6] could explain only partially their peculiar properties and further investigation appeared to be necessary. The most suitable method for that was judged to be impedance spectroscopy (IS) which,

* Corresponding author. Tel.: +30-331-7723277; fax: +30-331-7723184.

E-mail address: gpaterma@central.ntua.gr (H.S. Karayianni).

00167-577X/02/$ - see front matter
PII: S0167-577X(01)00459-1

alone or together with other methods, has been applied for investigating complex microstructures of solid materials [20] since it is sensitive to separate effects of the bulk material, grain boundaries and electrode interfaces. Ni deposits were examined by an impedance spectroscopy Q-meter method at a–c frequencies 8–22 MHz [21]. Although the results were significant, they failed to reveal the structural characteristics responsible for their behaviour. In the present work, Ni deposits were examined by an improved IS method in a region of lower frequencies, 1 Hz–100 kHz, where suitable information could be obtained. The microstructure of Ni electrodeposits was examined by electron microscopy. Then, a general model for their microstructure, consistent with the results of IS, was formulated, which may apply to explain the peculiar properties of Ni electrodeposits.

2. Experimental

The experimental configuration, materials, procedure, bath temperature of 50 °C, stirring rate of 1200 rpm and charge density of 146.3 C cm^{-2} employed for the preparation of Ni deposits on brass circular plates, 32 mm in diameter and 3.5 mm in height, in 1.22 M $NiSO_4$ and 1.22 M $NiCl_2$ baths, were the same as previously done [4]. Different pH values, 2–4.5, and current densities, 0.2–10 A dm^{-2}, were employed. With an electrochemical efficiency of 100%, the above charge density produces a 50-μm thick compact Ni deposit. The real thickness of the $NiSO_4$–Ni deposits (compact material) [4] and the equivalent to compact thickness of the $NiCl_2$–Ni deposits (porous material) [4] examined by IS were determined from their masses (Table 1).

The deposits were circular films 27 mm in diameter. These were detached carefully from substrates to avoid damage to their structure. Two platinum circular plate electrodes, 10 mm in diameter, were attached to both face surfaces of each deposit so that the three centres of circular plates coincided. The diameter of deposit (27 mm) is much higher than that of electrodes (10 mm) and so no edge correction was needed [22].

An improved IS method was employed by which a full spectrum of impedance values at 400 discrete successive frequency values between 1 Hz and 100 kHz is obtained within a short time interval of the order of 1 s, allowing the detection of small spectrum details not distinguishable with common methods (i.e. the Q-meter method, etc.). Impedance measurements were obtained with a low-frequency Dynamic Signal Analyser (DSA) (Hewlett-Packard model 3561A). The instrument measured simultaneously the amplitude of the impedance vector ($|Z|$) and the phase (φ) shift at each frequency (F). A

Table 1
Values of R_a, R_b and C_a of the Ni electrodeposits prepared in $NiSO_4$ and $NiCl_2$ electrolyte baths at different pH and j values with different thicknesses

Electrolyte	pH	j (A m^{-2})	Ni thickness (μm)	$10^3 \times R_a$ (Ω)	$10^3 \times R_b$ (Ω)	$C_a \times 10^4$ (F)
$NiSO_4$	4.0	0.2	45.8	36.9	1.4	2.2
	4.0	1.2	49.4	37.1	1.4	2.2
	4.0	3.5	44.1	38.1	3.7	2.2
	4.0	4.0	43.0	34.8	3.5	2.4
	4.0	5.0	43.6	36.9	1.3	2.2
$NiCl_2$	2.0	0.9	47.4	36.8	1.4	2.3
	2.5	1.0	43.1	34.6	3.5	2.4
	2.5	3.0	45.0	35.4	3.3	2.3
	2.5	5.0	47.6	37.5	1.4	2.2
	3.0	7.0	48.0	34.8	3.4	2.4
	4.0	1.2	48.0	34.7	3.5	2.4
	4.0	2.5	47.0	35.1	3.5	2.4
	4.0	4.0	48.3	34.7	3.4	2.4

periodic noise signal (large number of sine-wave signals) was applied by the instrument to the system composed of the sample combined in series with a constant, known resistance. The voltage across the resistance was kept less than 10% of the total voltage applied to the terminals to minimise its effect on φ. The real and imaginary parts of Z ($\mathrm{Re}Z$ and $\mathrm{Im}Z$, respectively) and conductivity (σ) were determined. Measurements were taken at room temperature. The microstructure of Ni electrodeposits was also examined by electron microscopy and suitable electron photomicrographs were obtained.

3. Results

3.1. Results of the impedance spectroscopy examination of Ni electrodeposits

The φ vs. frequency plots of the $NiSO_4$–Ni and $NiCl_2$–Ni deposits prepared at different pH and current density (j) values are shown in Fig. 1. The real part of impedance (Z) and imaginary part of impedance, (Z) vs. F plots are shown in Fig. 2a,b. All plots relevant to the different $NiSO_4$–Ni or $NiCl_2$–Ni deposits essentially coincide. Appreciable differences appear only between the groups of $NiSO_4$–Ni and $NiCl_2$–Ni deposits. $\mathrm{Im}Z$ gives a maximum at an F_{max} which, to a good approximation, is 19.25 kHz for all cases.

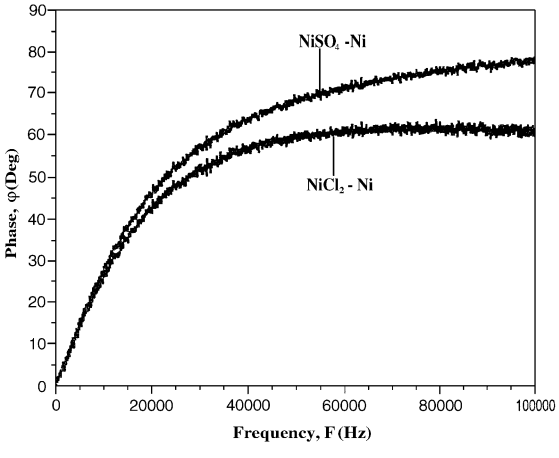

Fig. 1. Dependence of φ on F for the $NiSO_4$–Ni and $NiCl_2$–Ni electrodeposits.

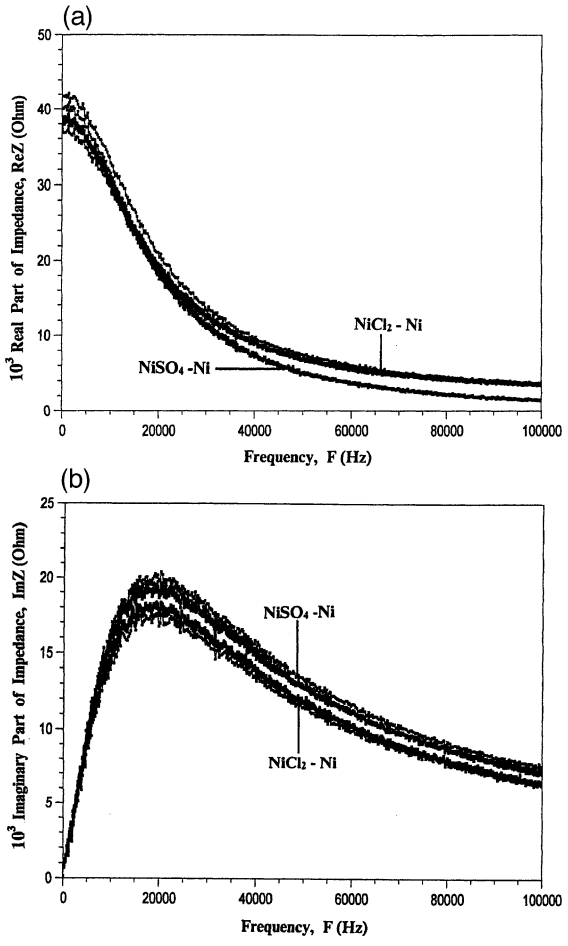

Fig. 2. Dependence of $\mathrm{Re}Z$ (a) and $\mathrm{Im}Z$ (b) on F for the $NiSO_4$–Ni and $NiCl_2$–Ni electrodeposits.

The corresponding Nyquist diagrams, i.e. the $\mathrm{Im}Z$ vs. $\mathrm{Re}Z$ plots (Fig. 3) are always almost perfect semicircles passing close to the origin. The centre of each semicircle lies almost on the $\mathrm{Re}Z$ axis. The semicircular $\mathrm{Im}Z$ vs. $\mathrm{Re}Z$ diagrams exclude the appearance of a self-inductance for $F \leq 100$ kHz [20]. The intersections of the semicircles with the $\mathrm{Re}Z$ axis are close to the $\mathrm{Re}Z$ values when $F \to 0$ and at $F = 100$ kHz. These values are noted as $R_a + R_b$ and R_b, respectively. The R_a and R_b values of all the $NiSO_4$–Ni and $NiCl_2$–Ni deposits are listed in Table 1. Always, $R_b \ll R_a$. Slight relative variations of R_a and significant ones for R_b are observed. The R_a's are essentially identical for all $NiSO_4$–Ni and $NiCl_2$–Ni deposits.

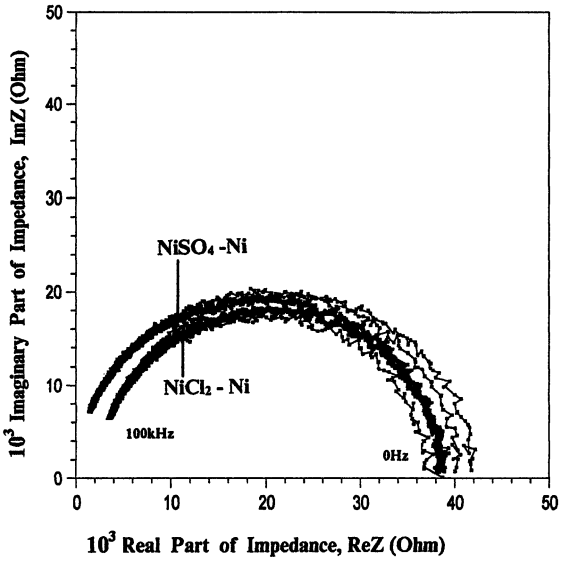

Fig. 3. The Nyquist diagrams for the $NiSO_4$–Ni and $NiCl_2$–Ni electrodeposits.

These Nyquist diagrams postulate an equivalent circuit consisting of the in parallel combination of R_a (resistive) and C_a (capacitive) elements combined in series with R_b (resistive) element [20] (Fig. 4) and that a single relaxation mechanism applies. Therefore

$$2\pi F_{max}\tau = 1, \quad (1)$$

where τ is the relaxation time. Because $F_{max} \approx 19.25$ kHz, it is inferred that $\tau = 8.27 \times 10^{-6}$ s. The F_{max} must also satisfy the equation [20]

$$2\pi F_{max} R_a C_a = 1. \quad (2)$$

The C_a values, found from Eq. (2), are given in Table 1. Both C_a's and R_a's are essentially independent of pH, *j*, electrolyte kind and, therefore, also of the texture axis [4].

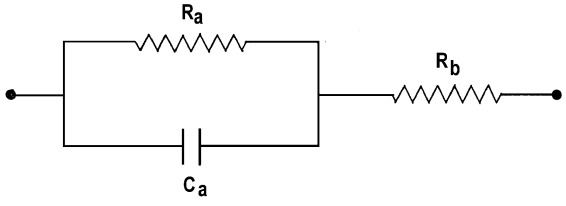

Fig. 4. The equivalent circuit for the Ni electrodeposits.

The a–c conductivity, σ, was calculated by the form

$$\sigma = 4h(\pi D^2)^{-1} G = 4h(\pi D^2)^{-1} \mathrm{Re}Z(|Z|^{-2}), \quad (3)$$

where *h* is the Ni deposit thickness, *D* is the diameter of platinum electrode and *G* is the conductance or the real part of the admittance Z^{-1}. The σ vs. *F* plots are shown in Fig. 5. Considering the conductivity of pure Ni, $\approx 1.28 \times 10^5\ \Omega^{-1}\ \mathrm{cm}^{-1}$ [23], and the results in Fig. 5, it appears that the Ni deposits loses their metallic character to a great extent.

The determined $F_{max} \approx 19.25$ kHz and $\tau = 8.27 \times 10^{-6}$ s cannot be attributed to a relaxation mechanism involving electron polarisation, ionic/atomic polarisation, dipole polarisation and space charge polarisation since these processes are met at $F \approx 10^{12}$–10^{13}, $\approx 10^8$–10^9, $\approx 10^6$ and $\approx 10^3$ Hz, respectively [24]. It could be assumed that the results of this study refer to the last case. However, exhaustive examination of Ni deposits by the XRD, optical microscopy and electron microscopy [4] did not reveal the presence of any other phase than Ni (see also later). Hence, there are not two or more discrete phases so that a space charge could be developed. Because τ is essentially constant, the species involved in the relaxation mechanism must be identical in all cases. Only hydrogen can satisfy that condition.

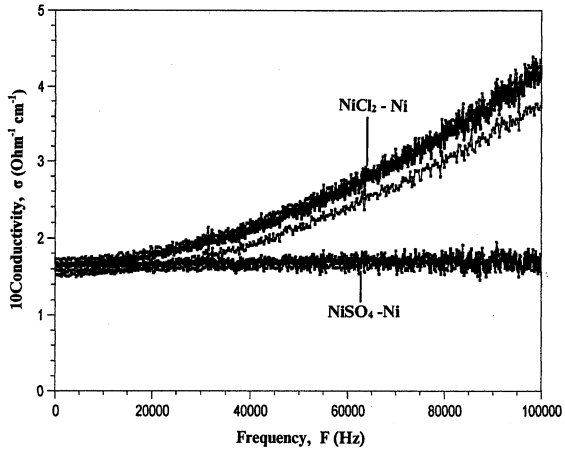

Fig. 5. Dependence of σ on *F* for the $NiSO_4$–Ni and $NiCl_2$–Ni electrodeposits.

The hydrogen atoms must participate in the conduction by a diffusion/hopping mechanism. It anticipates an activation energy comparable to that of hydrogen diffusion inside Ni. Similar relaxation mechanism was also revealed for Cu deposits containing hydrogen [25]. As shown [25], τ and the diffusion coefficient (D) are related by the equation

$$\tau = a^2/(12D)^{-1}, \quad (4)$$

where a is the lattice constant of the solid material. For the Ni lattice, $a = 3.5238$ Å [24]. From the τ and a values, D is found to be $D = 1.25 \times 10^{-11}$ cm^2 s^{-1} at room temperature. It agrees well with that found by other methods for Ni deposits (implanted with P) $2–8 \times 10^{-10}$ [26,27] and Ni (melt-quenched $Ni_{81}P_{19}$ amorphous alloy) 2.2×10^{-11} cm^2 s^{-1} [28] at this temperature verifying the above analysis.

3.2. The microstructure of Ni electrodeposits

The microstructure of $NiSO_4$–Ni and $NiCl_2$–Ni deposits was examined by electron microscopy. As verified, it is complex affected relatively slightly by pH and strongly by j in both cases. The microstructure of the $NiSO_4$–Ni and $NiCl_2$–Ni deposits in some characteristic cases is shown in Figs. 6 and 7.

The $NiSO_4$–Ni deposits (Fig. 6) are compact materials although micropores may appear. In general, the crystals/grains of material surface tend to be developed according to a pyramidic structure (a–d), but finally, it is transformed to a structure made of densely packed agglomerates of hemispherical grains, separate grains and clusters. The SO_4^{2-} ions in the

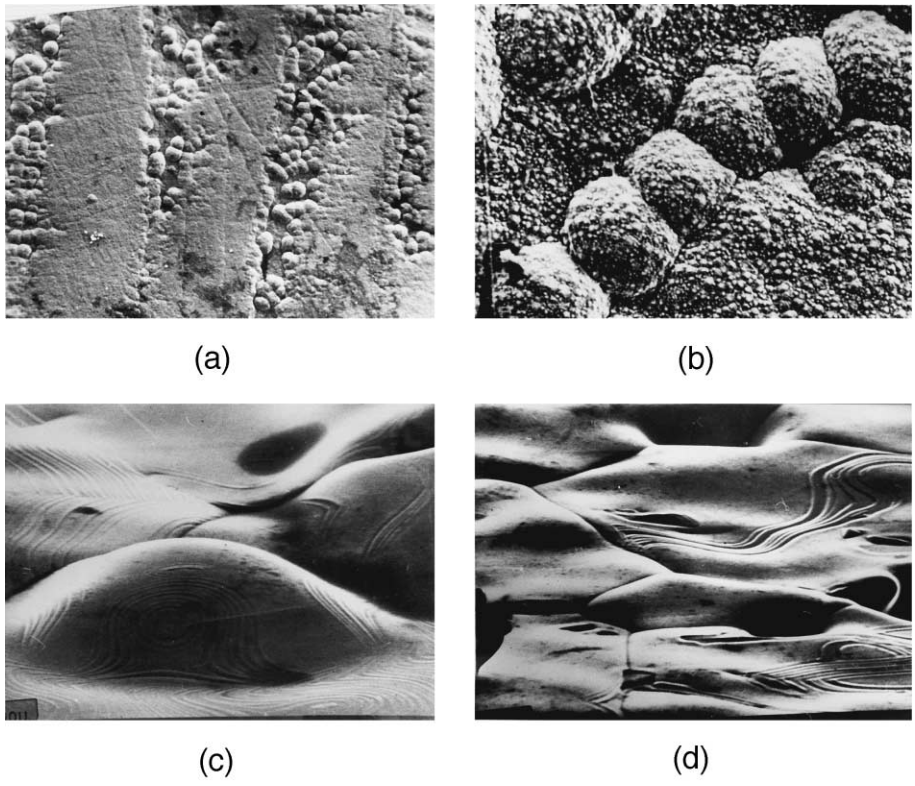

Fig. 6. Electron microscopy photomicrographs for the surfaces of $NiSO_4$–Ni deposits obtained at $j = 2$ (a and b), 3.5 (c) and 10 (d) A dm^{-2}; pH = 2 (a and b), 3.5 (c) and 4.5 (d). (a) Secondary electron image (SEI) × 60, (b) SEI × 480, (c and d) Scanning electron microscopy (SEM) × 4000.

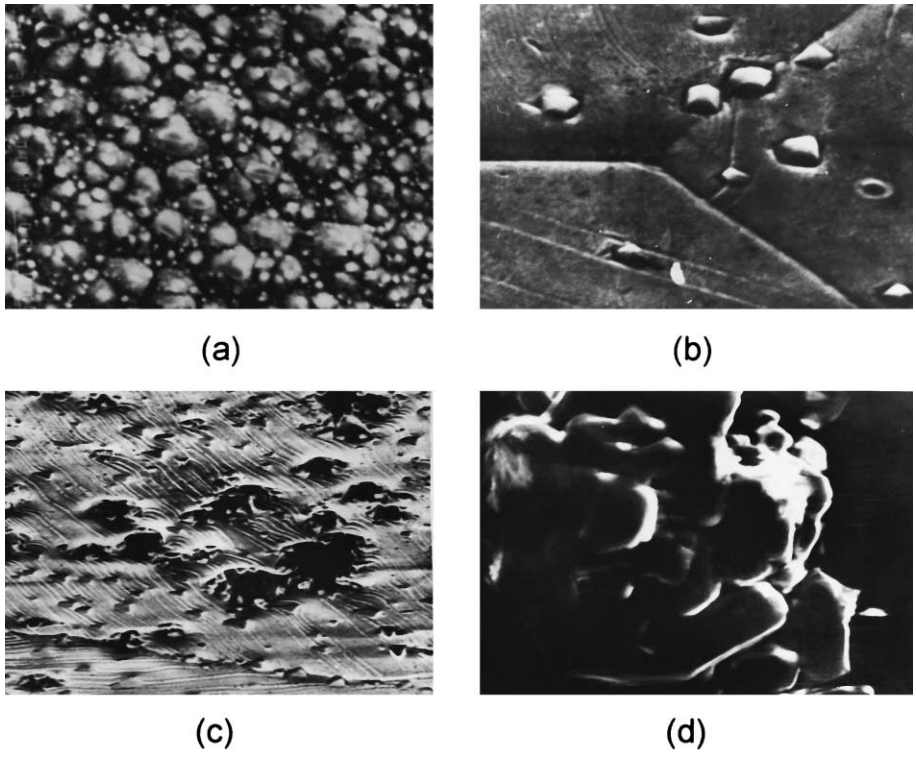

Fig. 7. Electron microscopy photomicrographs of the surfaces (a–c) and of a section (d) of $NiCl_2$–Ni deposits obtained at $j = 0.3$ (a), 1.5 (b), 1.9 (c) and 2.5 (d) A dm^{-2}; pH = 3 (a, b and d) and 4 (c). (a) SEI × 3000, (b) SEM × 4000, (c) SEM × 1500, (d) SEM × 480.

bath solution act like a surfactant on the corners and edges of pyramids, which would appear, and they become spheroidised. The simultaneous evolution of H_2 [4] acts similarly.

At low and intermediate j's, a columnar structure, parallel to gravity during the growth of deposits, is verified (Fig. 7a). Between columns of a flat material developed almost uniformly, linear valleys enlarged upwards appear inside, in which separate grains or clusters exist (Fig. 6a,b). The first regions are those at which the development of attached H_2 bubbles during the Ni deposition process is not favoured. In the second ones, despite the vigorous bath stirring, their development may be favoured hindering the Ni deposition and H_2 evolution processes until the bubbles are detached. Since the H_2 evolution rate is low [4], the average H_2 bubble grows slowly, remaining attached for a relatively long time before its detachment. When detached, the bubbles move spontaneously upwards. Small bubbles detached from lower surface regions may be joined with bubbles attached at upper positions forming larger attached ones. As a result, valleys are thus formed which are generally enlarged upwards.

At intermediate and high j's, a fine microstructure and a stepwise sub-microstructure are verified (Fig. 6c,d). The observed stepwise sub-microstructure may be due to a stepwise development of each pyramid or is created by hydrodynamic effects of the vigorously stirred bath. The pyramidic/spheroidised structure is favoured at low and intermediate j and pH values, where the relative rates of H_2 evolution are high [4] (Fig. 7a–c). At high j and pH values, where the relative rates of H_2 evolution are low [4], besides the pyramidic/spheroidised structure, a cellular structure is also favoured (Fig 7d).

The only distinguishable phase in Fig. 6 is that of Ni. Nevertheless, separate dark regions in the boundaries between two and mainly between three neighbouring grains are distinguished (Fig. 6b–d), which

are attributed primarily to inclusions and secondarily to void spaces. Such regions are also dispersed on the surface of grains. The latter regions are destined to become the boundary regions containing inclusions and/or voids between neighbouring grains as above during the next stages of Ni deposition process. Such regions are rare or absent inside the bulk of each separate grain.

The $NiCl_2$–Ni deposits (Fig. 7) are fine spongy materials (Fig. 7a,c,d). Their structure also tends to become a pyramidic/spheroidised one at low j's, Fig. 7a. A stepwise sub-microstructure is also verified at intermediate j's (Fig. 7b,c). This stepwise sub-microstructure is explained as for the $NiSO_4$–Ni deposits. At intermediate j's, the material shows a clear pyramidic structure (Fig. 7b). The boundaries between two neighbouring coarse pyramids are distinguished in the lower region of Fig. 7c.

The growth of crystallisation nuclei on the surface of the big pyramids (Fig 7b,c) predicts a dentritic development of material. Pores of largely varying sizes are observed in each grain (Fig. 7c) created probably by the dentritic development "per se" and/or by the adsorption of H_2. At higher j's, a porous, columnar, spongy and dentritic microstructure is clearly shown (Fig. 7d) which seems to be characteristic for the $NiCl_2$–Ni deposits. The average grain sizes of $NiCl_2$–Ni deposits is generally lower than that of the $NiSO_4$–Ni deposits.

The only distinguishable phase in Fig. 7 is also that of Ni. However, as in the $NiSO_4$–Ni deposits, separate dark regions in the boundaries between two and mainly between three neighbouring grains as well as on the surface of the grains appear, which are attributed to the same reasons, i.e. to inclusions and voids. The number and extent of such regions in the $NiCl_2$–Ni are larger than in the $NiSO_4$–Ni deposits. This is also valid for the bulk grains.

4. Discussion

4.1. Interpretation of the involvement of hydrogen in the mechanism of conduction

The adsorption of hydrogen on metallic surfaces disturbs the band structure of the metals affecting the electrical conductivity. An increase of conductivity was observed during the adsorption of hydrogen on some metallic surfaces [29] but even metal–insulator transitions occurred in other cases [29]. Although the mechanism of its adsorption is generally different from that of its incorporation in the metal bulk, e.g. in Ni deposits forming hydrides [8], these are consistent with the decrease of conductivity of Ni deposits.

Because the H atoms are small and mobile, they can be incorporated easily in interstitial positions (H) and voids (H and/or H_2). The formation of H^- is possible because the electronegativity of H is appreciably higher than that of Ni. That is why Ni hydride is easily formed [8]. Electrons are captured from those in the conduction band of Ni causing the decrease of conductivity. The ionised H atoms contribute to the conduction mechanism by their hopping/diffusion through voids or interstitials causing some increase of conductivity. The final result is a strong decrease of conductivity of Ni deposits, as indeed observed. The H_2 molecules must be incorporated mainly in voids in the grain boundaries. The probable incorporation of non-ionised H atoms must decrease the conductivity due to both the deformation of the crystal lattice and disturbance of the Ni band structure.

4.2. Interpretation of the ohmic R_a and R_b and capacitive C_a elements

The size of SO_4^2 incorporated in the $NiSO_4$–Ni deposits [4,7] is much larger than that of Ni^{2+}, and SO_4^{2-} cannot penetrate the Ni crystal lattice. They can be incorporated exclusively in the grain boundary surfaces, where they are strongly bound by ionic bond and become immobile. The Ni^{2+} bound with SO_4^{2-} do not offer electrons to the conduction band. The formed $NiSO_4$ is an insulator increasing the resistance of Ni deposits.

The Cl^- ions, present at significant amounts inside the $NiCl_2$–Ni deposits [10], and OH^- must be located also mainly in these surfaces as impurities. Ni^{2+} are bound with Cl^- and OH^- by ionic bond. The formed $NiCl_2$ and $Ni(OH)_2$ or Ni(OH) [9–13] are also insulating materials increasing the resistance of deposits. The existence of Cl_2 in the grain boundaries exerts similar effects.

The H_2 molecules incorporated mainly in the grain boundaries in both the $NiSO_4$–Ni and $NiCl_2$–Ni

deposits act as a physical and energy barrier and exert similar effects.

Hence, all the above inclusions increase strongly the resistance of the grain boundary surfaces. In some places of these surfaces, the concentration of the insulating impurities and their thickness become sufficiently high and this part of the surfaces does not permit the current passage, either electronic or by the hydrogen diffusion/hopping mechanism; it is essentially an insulator and becomes capacitive. The C_a capacitive element is thus justified. Even the H_2O molecules, probably embodied in the above surfaces, give a capacitive character to these surfaces due to their high dipole moment. It is noted that the geometrical self-capacitance of Ni deposits may imperceptibly contribute to C_a.

In the remaining part of the grain boundary surfaces, the concentration of the insulating impurities and their thickness are not significant and it behaves as an ohmic resistance. The passage of electronic current through this part is strongly hindered but possible, while the current passage by the hydrogen diffusion/hopping mechanism becomes significant compared to the electronic one. The R_a ohmic element is attributed to that part of the grain boundary surfaces. Apparently, C_a and R_a are combined in parallel.

The imperceptible variations of C_a and R_a with the preparation conditions and the kind of electrolyte can be interpreted if it is considered that the above two parts of the grain boundary surfaces are comparable in the different cases. This is possible considering that the capacitive regions are mainly the boundaries between three grains, where impurities at large amounts are accumulated, and the ohmic regions are mainly those between two grains where the amount of inclusions are much lower.

The grains bulk must also have some resistance R'_b, much lower than R_a mainly because the amount of inclusions is negligible compared to that of the ohmic part of the grain boundaries. The conductivity inside them must approach that of pure Ni. Therefore, R'_b must be much lower than R_b, or it is a part of R_b. The remainder $R_b - R'_b$ is attributed to arbitrary resistances in the contacts between specimens and electrodes. This justifies the significant variation of R'_bs, which is thus attributed to the scatter of these resistance values.

4.3. Interpretation of the variation of σ with F and the kind of electrolyte

Due to the forced electrochemical process of Ni deposition, the sizes of grains become generally small and a significant concentration of lattice defects of both kinds, interstitials and voids exists inside them. Since the $NiCl_2$–Ni are porous, spongy and dendritic materials [4] and have more kinds and higher amounts of inclusions than the $NiSO_4$–Ni, the $NiCl_2$–Ni have lower crystallite sizes, more kinds and higher concentrations of defects than the $NiSO_4$–Ni; the crystal lattice of $NiSO_4$–Ni approaches better the perfect crystal lattice.

The participation of hydrogen atoms by the hopping mechanism in the conduction can explain the variation of σ with F for both $NiSO_4$–Ni and $NiCl_2$–Ni. It is known [30] that three cases of the hopping conduction mechanism are distinguished. The first is a simple hopping mechanism where, in the absence of long range interactions, a single particle (H^- in the present case) is presumed to move along an infinite lattice of identical potential wells. The conductivity is then expected to be relatively low and independent of F. This case is met in the $NiSO_4$–Ni, the crystal lattice of which approaches the perfect crystal lattice and the potential wells in it are more regularly distributed.

In the second case, double potential wells separated by a barrier with height lower than that of the outer wells walls (single biwell potential) exist, and a single particle hopping is supposed to occur forward and backward inside each double potential well. The conductivity may increase with increasing rate of F, and the σ vs. F plots stem from a relatively low value on the σ axis. The double potential wells may be anticipated by the lattice structure or are formed by suitable defects. In the third case, triple potential wells exist in which the heights of the two internal potential barriers are not equal and both are lower than the lateral equal potential barriers. A single particle hopping is supposed to occur forward and backward inside them. In this case, a stepwise, constant low σ appears in the region of low F's, followed by an accelerated increase of σ, followed by a stepwise, constant σ, etc. Such potential wells may be anticipated by the crystal lattice or are formed by suitable complex defects.

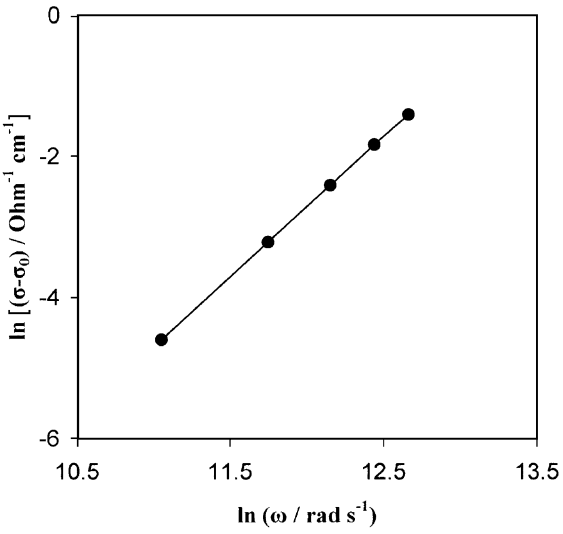

Fig. 8. Plots of $\ln(\sigma - \sigma_0)$ vs. $\ln \omega$ for the $NiCl_2$–Ni deposits.

The conductivity of $NiCl_2$–Ni must be attributed to the second case or to a mixture or a hybrid between the first and the second cases. This may be also attributed to a mixture or a hybrid between the first, second and third cases, where in the third case, the first stepwise stage appears for a narrow range of F's in the vicinity of $F = 0$. Nevertheless, the successive stage, where the conductivity increases, normally develops. The second and probably the third cases are possible mainly for $NiCl_2$–Ni rather than for $NiSO_4$–Ni. This is due to the much higher amount of inclusions, the porous structure, the lower grain sizes, etc. of $NiCl_2$–Ni, which create complex defects capable of forming such double and probably triple potential wells, mainly near the grain boundaries. It is noted that σ in the second case, as well as in the third case, supposing that the first stepwise conductivity stage appears in the vicinity of $F = 0$ and in a narrow range of F's, is given by the form [30].

$$\sigma = \sigma_0 + A\omega^n \text{ or } \ln(\sigma - \sigma_0) = \ln A + n\ln\omega, \quad (5)$$

where σ_0 is σ at $F = 0$, A and n are constants, characteristic of the material, and ω is the cyclic frequency. To test its validity, the average σ's of the $NiCl_2$–Ni were determined at various discrete F's like 20, 40, 60, 80 and 100 kHz and the $\ln(\sigma - \sigma_0)$ vs. $\ln \omega$ plot was constructed (Fig. 8). By the linear regression analysis, the n, A and correlation coeffi-

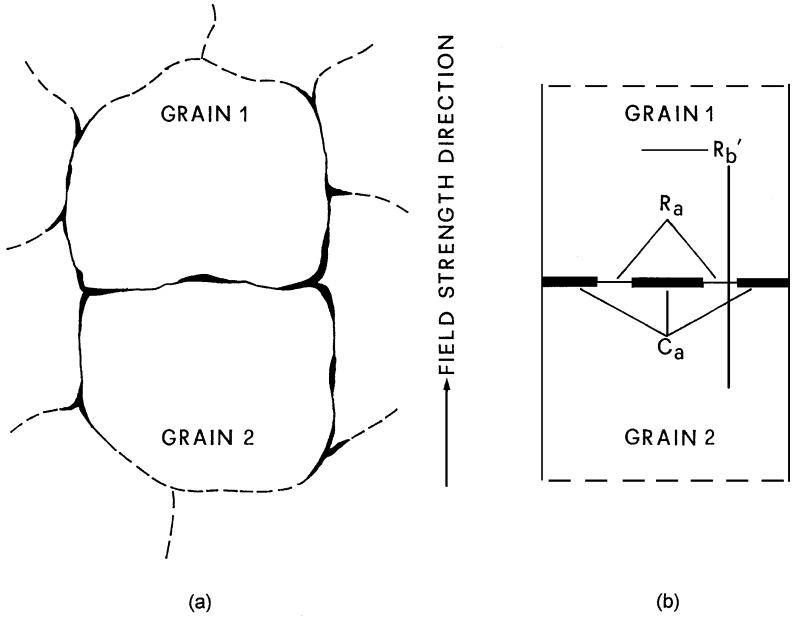

Fig. 9. Real (a) and idealized (b) schematic representations of the boundaries between two grains. The regions of the ohmic resistance R_a and capacitance C_a of the grain boundaries and of the ohmic resistance R'_b of the grains bulk are depicted.

cient values were found to be 1.9898, ≈ 2, 2.852×10^{-12} and ≈ 1, respectively, verifying Eq. (5) and the whole above analysis.

4.4. The suggested model for the microstructure of Ni electrodeposits

As verified, the microstructures of $NiSO_4$–Ni and $NiCl_2$–Ni are complex enough, while a large variety and strongly variable quantities of inclusions exist in the deposits [4–13]. Due to the complex nature/composition and structure of deposits, which are largely varying with the kind of bath solution and preparation conditions, a general and satisfactory interpretation of the peculiar properties of Ni electrodeposits [14–19] based on these characteristics seems to be extremely difficult or impossible. Nevertheless, the IS results showed that the role of the grains and inclusions is similar in both $NiSO_4$–Ni and $NiCl_2$–Ni deposits. This allows the formulation of a general model for the microstructure of Ni deposits applicable in both cases, which may be used to explain the peculiar properties of Ni electrodeposits in future studies.

Taking into consideration all given above, a real and an idealized schematic representation/model of the bulk and boundary surfaces of two grains, with their boundary surface perpendicular to the field strength direction, the ohmic resistances and capacitance regions and the corresponding elements of the equivalent circuit are given in Fig. 9a,b. This model is applicable irrespective of the complexity of the microstructures and the kinds and quantities of inclusions for both the $NiSO_4$–Ni and $NiCl_2$–Ni deposits.

5. Conclusions

(1) The inclusions yield capacitive regions in the boundaries mainly between three grains, and ohmic regions mainly between two grains. The conduction through the latter regions embraces a hopping/diffusion mechanism of incorporated ionised H atoms.

(2) The conductivity of $NiCl_2$–Ni is generally higher than that of $NiSO_4$–Ni for $F \gg 0$, which is well justified by the hydrogen hopping/diffusion mechanism of conduction.

(3) The diminution of the conductive–metallic character of Ni deposits, the incorporation of highly resistive or insulating species in the grain boundaries, the hydrogen hopping/diffusion conduction mechanism, the equivalent circuit (Fig. 4) and the microstructure model (Fig. 9) may explain in future studies the peculiar properties of Ni deposits [14–19].

(4) The results of this study are important, stimulating further investigation for the mechanism of current conduction through the Ni electrodeposits and their microstructure.

References

[1] J. Amblard, G. Froment, G. Maurin, Electrodeposited Surf. 2 (1974) 205.
[2] J. Amblard, G. Maurin, D. Mercier, N. Spyrellis, Scr. Metall. 16 (1982) 572.
[3] J. Amblard, G. Froment, N. Spyrellis, Surf. Technol. 5 (1977) 205.
[4] H.S. Karayianni, G. Patermarakis, Electrochim. Acta 40 (1995) 1079.
[5] A.K.N. Reddy, J. Electroanal. Chem. 6 (1963) 141.
[6] G. Maurin, Oberfache-Surf. 11 (1970) 297.
[7] J. Amblard, G. Froment, G. Maurin, N. Spyrellis, "Extended Abstract" No. 469, Fall Meeting of the Electrochemical Society, San Diego, CA, October 19–24, vol. 86-2, 1986, pp. 700–701.
[8] S. Nakahara, E.C. Feleder, J. Electrochem. Soc. 129 (1982) 45.
[9] I. Epelboin, M. Jousselin, R. Wiart, J. Electroanal. Chem. 119 (1981) 61.
[10] R.P. Slizys, Proc. of the 10th Lithuanian Conf. of Electrochem., 1988, p. 26.
[11] M. Schlotter, Trans. Faraday Soc. 31 (1935) 1177.
[12] M. Jousselin, These de 3eme cycle, Paris, 1981.
[13] I. Epelboin, R. Wiart, J. Electrochem. Soc. 118 (1971) 1577.
[14] C.S. Karayianni, P. Vassiliou, in: L. Margantis (Ed.), Proceedings of the 3rd Balcan Conference on SEMicroscopy and Microanalysis, Athens, September 1989. Athens University Press, Athens, 1989, p. 255.
[15] H. Karayianni, N. Amandi, P. Vassiliou, J. Mater. Sci. Lett. 13 (1994) 503.
[16] Th. Skoulikidis, S. Polymenis, A. Kostoudi, Mol. Cryst. 158 (1988) 197.
[17] M. Koui, H.S. Karayianni, M. Kartsonakis, Liq. Cryst. 22 (1997) 567.
[18] A. Brenier, C.W. Jennings, Plating 35 (1948) 452.
[19] W.L. Pinner, B.B. Knapp, M.B. Diggin, in: F. Lowenheim (Ed.), Modern Electroplating. 3rd edn., Wiley, New York, 1975, pp. 260–341.
[20] J.E. Bauerle, J. Phys. Chem. Solids 30 (1969) 2657.

[21] H.S. Karayianni, G. Patermarakis, J.C. Papaioannou, J. Mater. Sci. 31 (1996) 6535.
[22] ASTM Designation: D/50-65/Tentative methods of test for A–C Loss characteristic and dielectric constant (permittivity) of solid electrical insulating materials.
[23] R.C. Weast (Ed.), Handbook of Chemistry and Physics. 60th edn., CRC Press, Boca Raton, FL, 1979.
[24] A. West, Solid State Chemistry and Its Applications. Wiley, New York, 1984, p. 537.
[25] I.-J. Yang, J. Electrochem. Soc. 138 (1991) 2086.
[26] R. Nishimura, R.M. Latanision, G.K. Humbler, in: R.B. Diegle, K. Hashimoto (Eds.), Corrosion, Electrochemistry and Catalysis of Metallic Glasses, vol. 88-1, The Electrochemical Society, Softbourg, 1988, p. 277, Proceeding Series, Pennington, NJ.
[27] R.L. Zeller, U. Landau, J. Electrochem. Soc. 137 (1990) 1107.
[28] R.M. Latanision, C.R. Compeau, M. Kurkela, in: R. Gibala, R.F. Heheman (Eds.), Hydrogen Embrittlement and Stress Corrosion Cracking. ASM, Metals Parks, OH, 1984, p. 297.
[29] D.M. Young, A.D. Crowell, Physical Adsorption of Gases, Butterworth, London, 1962.
[30] J. Ross Mac Donald (Ed.), Impedance Spectroscopy, Wiley, New York, 1987, p. 48.